Published online 10 February 2012 *Nucleic Acids Research, 2012, Vol. 40, No. 11* ***4925–4932***
doi:10.1093/nar/gks069

Force spectroscopy reveals the DNA structural dynamics that govern the slow binding of Actinomycin D

Thayaparan Paramanathan[1], Ioana Vladescu[1], Micah J. McCauley[1], Ioulia Rouzina[2] and Mark C. Williams[1,*]

[1]Department of Physics, Northeastern University, Boston, MA-02115 and [2]Department of Biochemistry, Molecular Biology and Biophysics, University of Minnesota, Minneapolis, MN-55455, USA

Received December 2, 2011; Revised January 18, 2012; Accepted January 19, 2012

ABSTRACT

Actinomycin D (ActD) is a small molecule with strong antibiotic and anticancer activity. However, its biologically relevant DNA-binding mechanism has never been resolved, with some studies suggesting that the primary binding mode is intercalation, and others suggesting that single-stranded DNA binding is most important. To resolve this controversy, we develop a method to quantify ActD's equilibrium and kinetic DNA-binding properties as a function of stretching force applied to a single DNA molecule. We find that destabilization of double stranded DNA (dsDNA) by force exponentially facilitates the extremely slow ActD-dsDNA on and off rates, with a much stronger effect on association, resulting in overall enhancement of equilibrium ActD binding. While we find the preferred ActD–DNA-binding mode to be to two DNA strands, major duplex deformations appear to be a pre-requisite for ActD binding. These results provide quantitative support for a model in which the biologically active mode of ActD binding is to pre-melted dsDNA, as found in transcription bubbles. DNA in transcriptionally hyperactive cancer cells will therefore likely efficiently and rapidly bind low ActD concentrations (~10 nM), essentially locking ActD within dsDNA due to its slow dissociation, blocking RNA synthesis and leading to cell death.

INTRODUCTION

Actinomycin D (ActD) is a DNA binding (1) small molecule with potent activity as an antibiotic (2) and anticancer agent (3). It is a neutral molecule that contains a planar tricyclic phenoxazone ring that intercalates dsDNA and two cyclic pentapeptide side chains (Figure 1a). ActD can intercalate between double stranded DNA (dsDNA) base pairs (4–8), bind to single-stranded DNA (ssDNA) (9–12) and can even 'hemi-intercalate' between the bases of a single DNA strand (13,14). Early studies found that once bound ActD dissociates slowly from dsDNA (4), with a component of its dissociation occurring on a time scale of ~1000 s. These studies attributed ActD's anticancer activity to this slow kinetics, and found it to be due to the slow fitting of its two highly stressed cyclic penta-peptide side chains into the DNA minor groove below and above the intercalated phenoxazone ring (4,15) (Figure 1b). The fitting into the groove is stabilized by hydrogen bonding of the ActD side chains to guanine bases (5–7), and associated with major DNA duplex deformations, such as strong bending (6,8), unwinding (6,16) and even base flipping (16,17). Duplex deformations are also driven by optimization of the tricyclic phenoxazone ring stacking with the 3′ faces of guanine (or adenine) residues in the opposite DNA strands (8,14,16). Competing models for the anticancer activity of ActD depend on the favored binding mode; Intercalation may inhibit replication by stabilizing dsDNA in front of the replication fork (8), while binding to destabilized duplexes such as transcription bubbles may inhibit DNA transcription (18–20), and ssDNA binding may directly stall the DNA polymerase (12). However, despite many years of study by a variety of methods and detailed knowledge of the relationship between DNA sequence, structure and the strength of ActD–DNA interactions, there is no consensus for any of these models and the reason for the selective anti-cancer activity of ActD at low concentrations remains unclear.

Here we develop a single molecule method using optical tweezers to probe the DNA structural dynamics as ActD binds. This method allows us to completely characterize

*To whom correspondence should be addressed. Tel: +1 617 373 7323; Fax: +1 617 373 2943; Email: mark@neu.edu
Correspondence may also be addressed to Ioulia Rouzina. Tel: +1 612 624 7468; Fax: +1 612 625 2163; Email: rouzi002@umn.edu

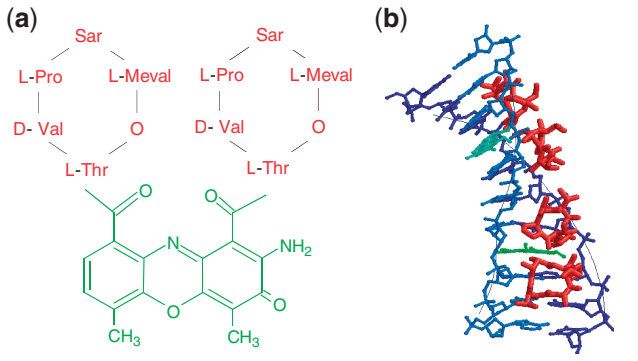

Figure 1. Actinomycin D structure and DNA interactions. (**a**) Chemical structure of ActinomycinD (ActD), with the planar phenoxazone ring system shown in green and pentapeptide side chains shown in red. (**b**) Ball and stick structure of two ActD molecules interacting with two DNA strands (different shades of blue) obtained from the pdb file IMNV, where phenoxazone rings (cyan for top molecule and green for bottom molecule) intercalate between DNA base pairs and the pentapeptide side chains (red) lie in the minor groove.

the kinetics and thermodynamics of ActD binding to a single polymeric dsDNA molecule as a function of force. In the optical tweezers experiments dsDNA is stretched by applying a force, F, to the polystyrene beads attached to its ends (Figure 2a). The beads are chemically attached to the opposite strands of the dsDNA such that it can freely rotate while stretching. As the dsDNA is stretched it is progressively destabilized by force until it undergoes a melting transition at force $F_m \sim 65$ pN (Figure 2b). During this transition the duplex DNA melts at essentially constant force, and progression into the transition reflects the increasing fraction of melted DNA base pairs. Above this transition force ($F > F_m$), stretching of predominantly ssDNA with a few remaining dsDNA regions is observed. Gradually releasing back the DNA retraces most of its stretching curve, signifying rapid re-annealing of the two melted DNA strands (at a pulling rate of 100 nm/s). This type of DNA force spectroscopy experiment makes ss or dsDNA substrates available for protein or ligand binding in a controllable way, and allows us to study the effects of these small molecules on either DNA state, as well as on the transition between them. Depending on the type of interaction, equilibrium and/or kinetic properties of binding can be characterized by stretching dsDNA in the presence of these small molecules (21). This approach has been successfully employed to characterize the equilibrium DNA interactions of rapidly binding duplex-stabilizing intercalators (22) as well as duplex-destabilizing ssDNA-binding proteins (23–25). A similar optical tweezers setup was used to quantify the slow dsDNA association kinetics of a novel threading intercalator (26).

In this study, we completely characterize the equilibrium binding as well as the extremely slow on and off kinetics of ActD binding to duplex DNA, which cannot be directly measured by conventional methods. The observed systematic facilitation of this ligand's on and off rates and dissociation constant by duplex destabilizing force allows extrapolation of these parameters to their force-free values. In addition, information on the structural changes in duplex DNA associated with the on and off processes as well as equilibrium binding are obtained. We find that ActD binding requires large dsDNA structural changes, which readily occur in a strongly destabilized DNA duplex that is functionally equivalent to two parallel single strands, but which are rare for stable dsDNA, resulting in much slower kinetics when the DNA is stable. The results allow us to propose a molecular mechanism for the anticancer activity of ActD based on the measured DNA structural dynamics. We use force spectroscopy in several complementary ways to obtain the same characteristics of ligand–DNA binding, rendering our conclusions definitive and self-consistent. This approach can be used as a general tool for studying the equilibrium and kinetic properties of small ligands and proteins that bind DNA slowly and non-cooperatively with measurable changes in DNA structure.

MATERIALS AND METHODS

The experiments described used a dual beam optical tweezers to stretch a single bacteriophage λ DNA molecule, end-labeled with biotin, between two streptavidin-coated polystyrene beads. After capturing a molecule, the surrounding solution was exchanged to obtain the desired concentration of ActD. The force-extension curves in the presence of ActD were then obtained at pulling rates of 100 nm/s and characterized according to the methods described in the manuscript. As these stretching experiments were observed to be out of equilibrium, a force clamp technique was also implemented to explore the slow ActD-binding process. During these constant force experiments DNA was stretched rapidly (~2 s) to a constant force and then maintained at that force using feedback. The feedback was obtained by measuring the change in force every second as the length changed in response to ligand association or dissociation. If this force was greater or less than the force setpoint by >1 pN, the force clamp adjusted the micropipette to a new position to maintain the force within 1 pN of the desired constant force value. These experiments were done while flowing the desired concentration of ActD through the cell (at a rate of ~100 μl/s). Once the extension reached equilibrium the ActD flow was stopped and buffer was flowed to wash out the ActD. The extension change during this rinse was also observed at constant force to characterize the dissociation kinetics. In principle, time constants as fast as 100 ms could be measured with this technique. However, in practice force-dependent binding at low forces before the setpoint is reached and the need to flow in a new solution with or without buffer limit the time constants we have measured to a few seconds or longer. To further check the effect of flow on the measured binding kinetics, control experiments first filled the cell with the desired concentration of ActD, followed by constant force measurements. All experiments were performed at 20°C, pH 7.5 and 100 mM Na^+.

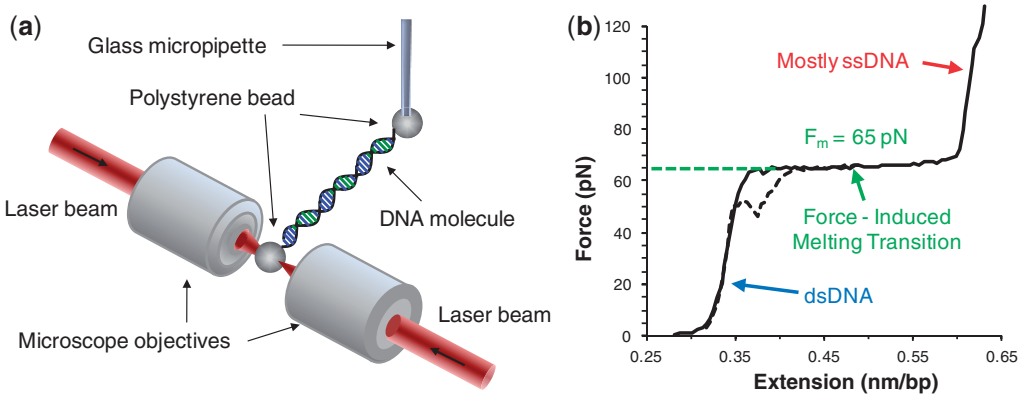

Figure 2. Stretching DNA with optical tweezers. (**a**) Schematic diagram of a dual beam optical tweezers instrument, which is used to trap and stretch single DNA molecules. (**b**) Typical force-extension curve obtained while stretching (solid curve) and releasing (broken curve) a single DNA molecule with optical tweezers at a pulling rate of 100 nm/s.

RESULTS

Limited available data (4,27–30) suggest that DNA duplex destabilization either by low salt, high temperature or DNA sequence mismatches leads to stronger and faster ActD–DNA binding compared to stable dsDNA. In order to test this hypothesis, we use a single molecule approach to destabilize dsDNA by applying a stretching force to its opposite ends with optical tweezers in the presence of ActD (Figure 3). The results below quantitatively demonstrate that DNA destabilization increases both the on and off rates of ActD, as well as its equilibrium DNA-binding affinity.

Non-equilibrium ActD–DNA binding observed in DNA stretching experiments

The DNA stretching curves in the presence of low concentrations of ActD ([ActD] < 100 nM) overlap the DNA stretching curves in the absence of the drug until the DNA is stretched into the melting transition, indicating that there is negligible binding at low ActD concentrations unless the dsDNA is destabilized (Figure 3a). Further stretching beyond the melting transition ($F > F_m$) shows an immediate effect of the drug, where the DNA length observed in stretching curves obtained in the presence of ActD appears shorter than those obtained without drug. The DNA release curves almost retrace the stretching curves above the melting transition, indicating that ActD–DNA binding is in equilibrium at these high forces. The most pronounced effect of ActD is that the DNA release curve after stretching through the melting transition does not match its stretching curve below melting transition ($F < F_m$) at our DNA pulling rate of 100 nm/s. The observed hysteresis indicates that ActD association to and dissociation from stable dsDNA at $F < F_m$ is much slower and weaker compared to unstable dsDNA at $F > F_m$. This result is further illustrated in Supplementary Figure S1, which shows increasing hysteresis in each DNA stretch-release cycle as DNA is progressively stretched further into its melting transition in the presence of 50 nM ActD. The observed hysteresis represents an increasing fraction of ActD-bound DNA complex that is proportional to the fraction of force-melted DNA and is locked within the duplex at $F < F_m$.

The strength of ActD binding to the two force-melted DNA strands at $F > F_m$ can be quantified as illustrated in Supplementary Figures S2a and S2b. At forces above the melting transition, $F > F_m$, the equilibrium DNA stretching curve shifts to smaller extensions as ActD concentration is increased from zero to ~75 nM. Fitting this DNA stretching curve at high forces as a weighted average between ActD-free ssDNA and ActD-saturated dsDNA yields the fractional ActD binding θ as a function of ActD concentration presented in Supplementary Figure S2b. The same stretch and release curves allow us to perform a complementary analysis that assumes the DNA release curve at $F < F_m$ after complete force-induced melting is the weighted average between re-annealed ActD-free dsDNA and ActD-saturated DNA. This analysis assumes that the same fractional ActD binding θ that was in equilibrium at $F > F_m$ becomes locked within the duplex at $F < F_m$. Fitting θ([ActD]) using both of these complementary methods with a simple expression for a non-cooperative two-state binding isotherm [described in the legend to Supplementary Figure S2 and similar to Equation (3) below] yields the ActD–DNA dissociation constant, $K_d(F > F_m) = 18 \pm 6$ nM. Our measured value of $K_d(F > F_m)$ is similar to the value of K_d ~10 nM measured previously for some specific sequence-mismatched DNA oligomers (10), supporting our hypothesis that dsDNA destabilization by either force or any other factor facilitates ActD binding. In addition to the use of stretching curves to obtain the equilibrium ActD–DNA binding affinity, the DNA pulling rate dependence of these curves can be used to estimate the kinetics of ActD–DNA binding at $F > F_m$ (see Supplementary Figure S3).

As ActD concentration is further increased (Figure 3b), the effect of the drug becomes prominent during stretching even at low forces below the melting transition ($F < F_m$), suggesting that higher ActD concentration leads to binding even to stable duplex DNA. However, the DNA stretch and release curves still do not overlap at low forces

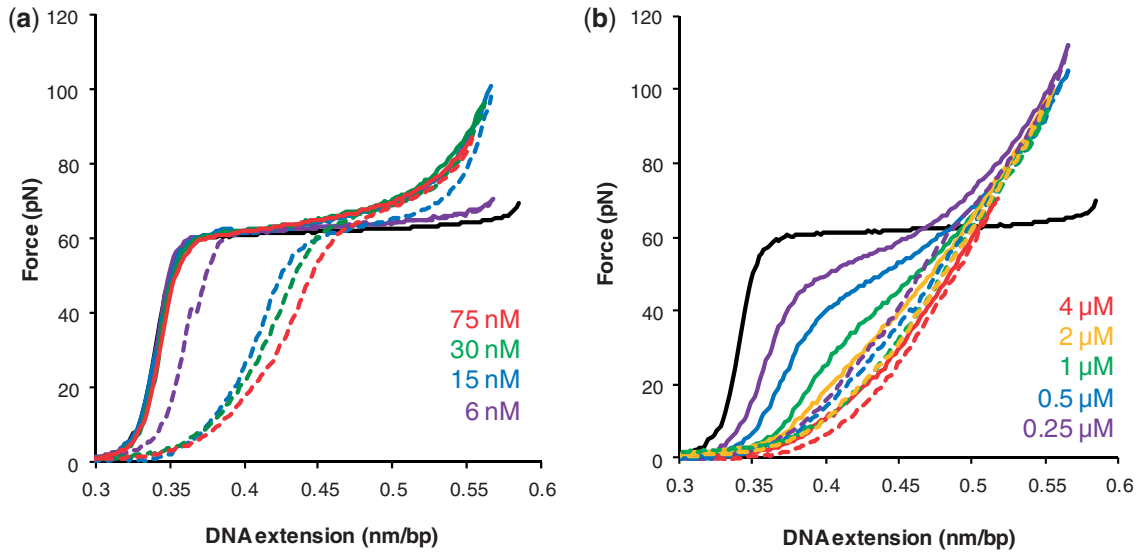

Figure 3. Stretching DNA in the presence of Actinomycin D. (**a**) DNA stretching (solid violet, blue, green and red) and releasing (corresponding broken curves) in the presence of low concentrations of ActD (6–75 nM) and in the absence of drug (black). The main features indicate that there is no sign of ActD binding until the DNA is stretched into the melting transition, while the hysteresis suggests association and dissociation are slower than the stretching time of 100 s. (**b**) DNA stretching (solid violet, blue, green, orange and red) and releasing (corresponding broken) curves in the presence of high concentrations of ActD (0.25–4 μM) and in the absence of drug (black). The results suggest faster binding to dsDNA at high concentrations, which saturates at [ActD] ~4 μM.

($F < F_m$) illustrating the non-equilibrium nature of the ActD–DNA complex and its slow on and off kinetics. The DNA stretching curve shows progressively more ActD binding until it converges with the DNA release curve at [ActD] ~ 4 μM. Analysis of the elastic properties of this saturated ActD–DNA complex (Supplementary Figure S4) suggests that it consists of two DNA strands strongly bound together at all forces by intercalated ActD, which we will denote ActD–2DNA hereafter. ActD–2DNA remains a rigid, well-defined structure that shows no signs of a melting transition, similar to saturated DNA complexes with more conventional intercalators (Supplementary Figure S4).

Measuring time-dependent ActD–DNA binding at constant force

The non-equilibrium DNA stretch and release curves observed below the melting transition ($F < F_m$) at 100 nm/s DNA pulling rate are expected to converge at some intermediate equilibrium curve as the DNA pulling rate is decreased to allow more time for ActD–2DNA complex association and dissociation. While we cannot pull slowly enough to directly observe this equilibrium ActD–DNA stretching curve, we can rapidly stretch or stretch and then release DNA to a particular force, and wait for the DNA extension to relax to equilibrium (Figure 4). Confirming our hypothesis, the DNA extension always converges to approximately the same equilibrium value, $x_{eq}(F, [\mathrm{ActD}])$, independent of the stretching history. Following the relaxation of the DNA extension $x(t, F, [ActD])$ to $x_{eq}(F, [ActD])$ with time at a constant force allows us to completely characterize the equilibrium affinity and kinetics of ActD–2DNA complex formation (Figure 5). Presented in Figure 5a are four $x(t)$ traces following ActD–DNA association as solution with 500 nM ActD is being flowed through the optical tweezers flow cell (open circles in Figure 5a). Fitting the $x(t)$ traces in Figure 5a to an exponential time dependence (solid curves in Figure 5a) yields the total relaxation rate $k_t = (k_{on} + k_{off})$ of ActD–2DNA and its equilibrium extension per basepair (x_{eq})

$$x(t) = x_{eq} + (x_0 - x_{eq}) \exp(-k_t t) \quad (1)$$

Determination of force-dependent equilibrium DNA-binding affinity

The fractional DNA binding with ActD, $\theta(F)$, at force F can be determined given the fitted $x_{eq}(F)$, ActD–2DNA extension $x_{sat}(F)$ (obtained from the ActD–DNA saturated curve in Supplementary Figure S4) and the known ActD-free dsDNA extension $x_{ds}(F)$:

$$\theta(F) = \frac{x_{eq}(F) - x_{ds}(F)}{x_{sat}(F) - x_{ds}(F)} \quad (2)$$

Using a simple binding isotherm, which assumes non-cooperative ligand binding to identical non-overlapping sites on DNA, the equilibrium dissociation constant $K_d(F)$ can be obtained:

$$K_d(F) = [ActD] \frac{1 - \theta(F)}{\theta(F)}. \quad (3)$$

This measured $K_d(F)$ decreases exponentially with force (Figure 5b), and can be fit to the expression

$$K_d(F) = K_d(0) \exp\left(-\frac{F \Delta x_{eq}}{k_B T}\right) \quad (4)$$

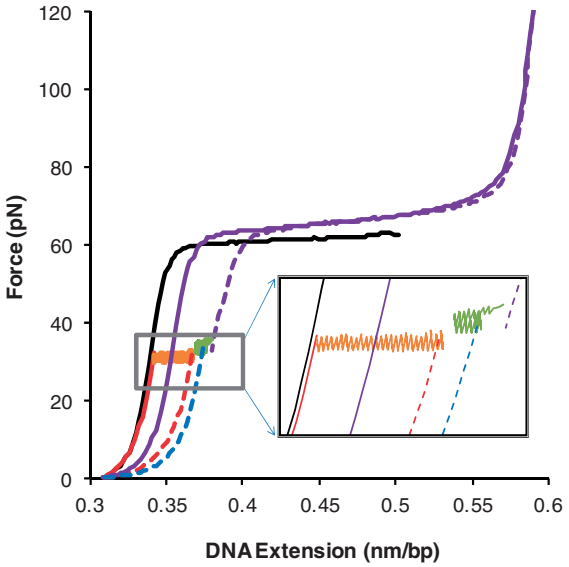

Figure 4. Equilibrium DNA extension at a given force reflects equilibrium ActD–2DNA binding and is independent of the DNA stretching history. DNA stretched rapidly in the presence of 50 nM ActD (red solid line) follows the naked DNA stretching curve (black) as ActD has no time to bind at this low concentration. The DNA is then held at a constant 30 pN force (orange) until it binds some ActD and elongates to an equilibrium extension and is then released back (red broken line). The same DNA is stretched through the melting transition (violet solid line) to form saturated ActD–2DNA complex and then released back to 30 pN (violet broken line), where it is held at a constant 30 pN force (green) until the excess of ActD–2DNA complex dissociates to reach much lower equilibrium binding, and the DNA is finally released back to the starting point (blue broken line). The inset is the magnification at the approximately constant 30 pN force measurement showing ActD–DNA binding from the under-bound state (trend of orange curve), and dissociation from the over-bound state (trend of green curve). These curves converge to almost the same equilibrium extension, which reflects equilibrium ActD–DNA binding for the given force and concentration.

to determine the dsDNA elongation associated with a single ActD–DNA binding event, Δx_{eq}, and the equilibrium dissociation constant in the absence of force, $K_d(0)$. Fitting yields $\Delta x_{eq} = 0.20 \pm 0.05$ nm, in the range expected for an intercalator (21), and $K_d(0) = 1.2 \pm 0.5\,\mu$M, which is similar to the value of $K_d \sim 3.5\,\mu$M for ActD–dsDNA binding obtained in previous solution studies (11). Extrapolation of the force dependence of K_d to high forces ($F \sim F_m$), suggests that K_d becomes close to the value measured independently at high forces $K_d(F > F_m) = 18 \pm 6$ nM as illustrated in Supplementary Figure S2.

Binding kinetics of ActD and DNA structural dynamics

Furthermore, $K_d(F)$ and $k_t(F) = k_{on}(F) + k_{off}(F)$ can be used to calculate individual ActD–DNA rates $k_{on}(F)$ and $k_{off}(F)$:

$$k_{on}(F) = \frac{k_t(F)}{1 + K_d(F)/[ActD]} \quad (5)$$

$$k_{off}(F) = \frac{k_t(F) \cdot K_d(F)/[ActD]}{1 + K_d(F)/[ActD]} \quad (6)$$

In deriving Equations (5) and (6) we assumed that $K_d(F) = [ActD](k_{off}/k_{on})$, i.e. that ActD–DNA association is non-cooperative and bimolecular. The bimolecular nature of ActD–DNA association is demonstrated by comparison of k_{on} values obtained in the presence of 50 nM (Supplementary Figure S5b) and 500 nM ActD (Figure 5c), showing a 10-fold difference in rates. It is also directly confirmed in a separate experiment in which we performed analogous DNA relaxation measurements at the fixed force $F = 30$ pN and several ActD concentrations (Supplementary Figure S6).

The ActD–2DNA on (green points in Figure 5c) and off rates (red and brown points in Figure 5c) at a particular concentration increase exponentially with the applied force:

$$k(F) = k(0)\exp\left(\frac{Fx}{k_B T}\right), \quad (7)$$

where k is either k_{on} or k_{off} and x is either x_{on} or x_{off}. Fits to the data (green and red line in Figure 5c) yield the rates in the absence of force $k_{on}(0) = (3.5 \pm 0.9) \times 10^{-4}$/s and $k_{off}(0) = (9.8 \pm 1.9) \times 10^{-4}$/s, which are in the range of rates measured in bulk studies (4,31,32). The off rate fit extrapolated to the high force limit agrees well with the range $0.004/\text{s} < k_{off} < 0.02/\text{s}$ estimated at high-force ($F > F_m$) from the pulling rate dependence of the DNA stretching curves (Supplementary Figure S3). In addition, these fits yield the length change required for a single ActD molecule to bind to or dissociate from DNA, $x_{on} = 0.33 \pm 0.03$ nm and $x_{off} = 0.11 \pm 0.02$ nm. The DNA elongation upon equilibrium ActD intercalation given by $\Delta x_{eq} = x_{on} - x_{off} = 0.33 - 0.11\,\text{nm} = 0.22\,\text{nm}$ agrees with $\Delta x_{eq} = 0.20 \pm 0.05$ nm within uncertainty, which was determined above from the force dependence of $K_d(F)$ using Equation (4) (Figure 5b). The off rates can also be independently obtained directly from the washing off experiments, where clean buffer is flowed through the cell to replace the ActD solution while holding the DNA at constant force (Supplementary Figure S7). The directly measured off rates (brown points in Figure 5c) agree very well with those given by Equation (6) (red points in Figure 5c).

We also obtained the force dependent bimolecular association rate $k_a(F)$ (Figure 5d) by combining force dependent measurements obtained at 50 nM (blue points), 500 nM (green points) and concentration dependent rates obtained at 30 pN (dark pink point). The exponential fit yields the zero force association rate $k_a(0) = (1.0 \pm 0.2) \times 10^3$/Ms. Very similar $k_a(0)$ values are obtained from analysis of the force $F_k([ActD], \nu)$ that promotes major intercalation of ActD into dsDNA at pulling rate $\nu = 100$ nm/s described in Supplementary Figure S8. The extrapolation of the force dependent bimolecular association rate $k_a(F)$ to high force ($F \sim F_m$) agrees well with the range of $2 \times 10^5/\text{Ms} < k_a(F > F_m) < 10^6/\text{Ms}$ obtained from the pulling rate experiments described in Supplementary Figure S3. Analogous control experiments performed in the absence of solution flow and in the presence of 50 nM ActD have shown the flow itself to have no effect on measured $k_a(F)$ or $k_{off}(F)$ (Figure 5c, d and Supplementary Figure S5b).

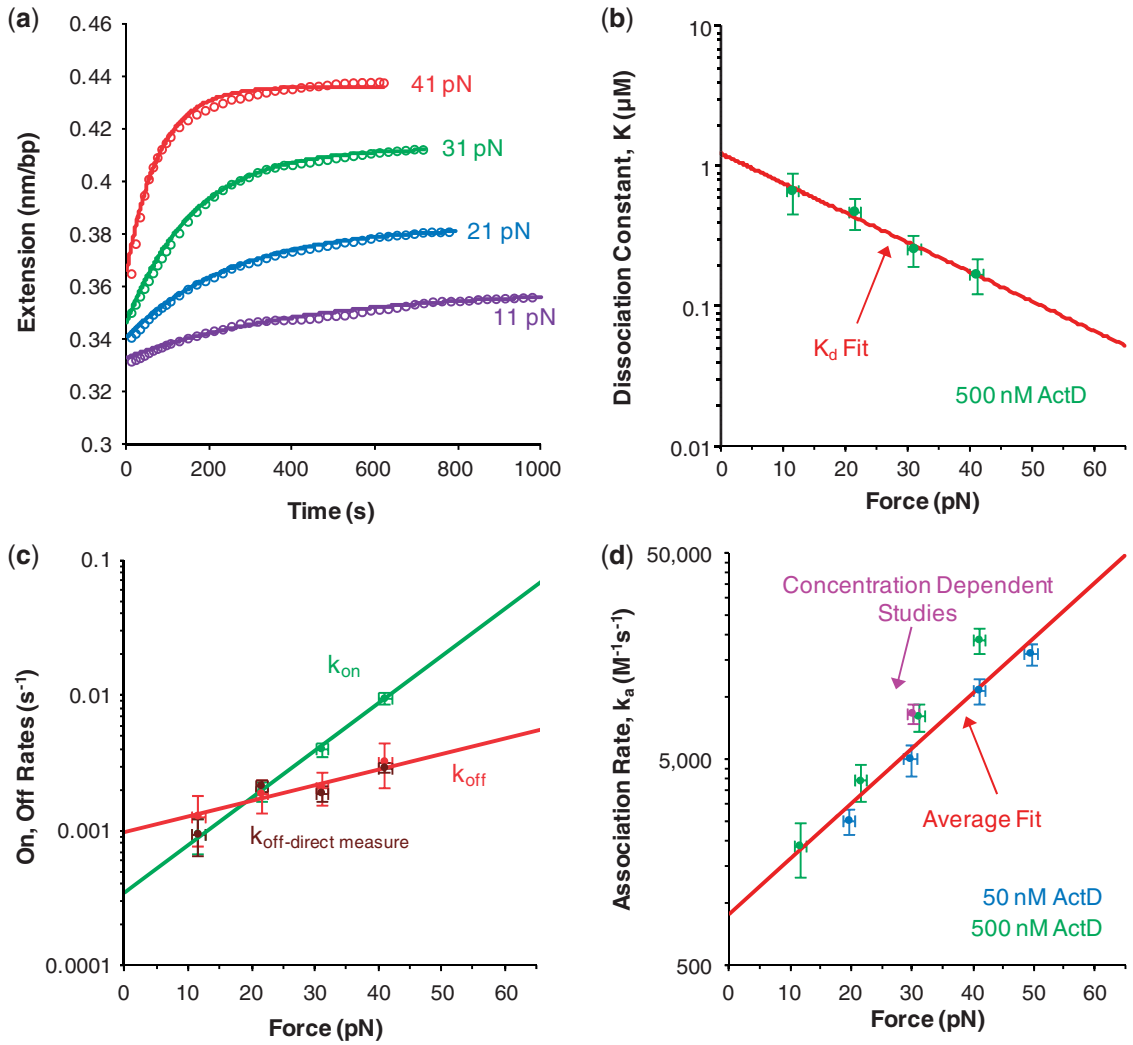

Figure 5. Relaxation of the DNA extension at constant force in the presence of ActD yields equilibrium binding properties and binding rates. (**a**) DNA extension as a function of time (open circles) and their exponential fits (lines) at constant force while flowing 500 nM ActD through the flow cell. (**b**) Force-dependence of the equilibrium dissociation constant, $K_d(F)$ in the presence of 500 nM ActD (green points) and the fit from Equation (4) with $\Delta x_{eq} = 0.20 \pm 0.05$ nm and $K_d(0) = 1.2 \pm 0.5$ μM (red line). (**c**) ActD–2DNA on (green points) and off (red points) rates calculated according to Equations (5) and (6), along with directly measured off rates (brown points) from Supplementary Figure S7. The green and red lines are fits to the on and off rates using Equation (7) with the parameters $k_{on}(0) = (3.5 \pm 0.9) \times 10^{-4}$/s, k_{off} $(0) = (9.8 \pm 1.9) \times 10^{-4}$/s, $x_{on} = 0.33 \pm 0.03$ nm and $x_{off} = 0.11 \pm 0.02$ nm. (**d**) Force dependence of the bi-molecular association rate constant $k_a(F)$ calculated using measured $k_{on}(F)$ values for 50 nM (blue points), 500 nM (green points) ActD, and concentration-dependent studies at $F = 30$ pN (pink point) discussed in Supplementary Figure S6. The solid dark red line represents an exponential fit to $k_a(F)$ corresponding to Equation (7) with $k_a(0) = (1.0 \pm 0.2) \times 10^3$/M s and $x_{on} = (0.25 \pm 0.02)$ nm.

DISCUSSION

The agreement of all of the ActD–DNA binding parameters measured in this study by several independent approaches confirms that ActD binds to and stabilizes two bound DNA strands via non-cooperative, bimolecular binding with very slow on and off rates. As the DNA stretching force is increased from 0 to ~65 pN, leading to progressive duplex destabilization, ActD–DNA binding becomes ~20-fold stronger (Figure 5b), while its on and off rates become ~100-fold and ~5-fold faster, respectively (Figure 5c). The fact that the DNA stretching force promotes both the ActD–2DNA on and off processes implies that the rate-limiting step for either event requires dsDNA lengthening. The DNA lengthening obtained from force dependent on rates, $x_{on} = 0.33 \pm 0.03$ nm, represents the large length change required for both intercalation and fitting of the penta-peptide side chains into the dsDNA the minor groove (Supplementary Figure S9). The structure then relaxes to $\Delta x_{eq} = 0.20 \pm 0.05$ nm, corresponding to the duplex elongation associated with ActD's phenoxazone ring intercalation as its side chain fitting is optimized. The additional DNA elongation $x_{on} - \Delta x_{eq} = 0.13 \pm 0.03$ nm is within error equal to the lengthening required to dissociate that is obtained from the force dependence of the off rates ($x_{off} = 0.11 \pm 0.02$ nm). This suggests that the DNA distortion required to remove the

side chains from the DNA minor groove during dissociation is similar to that required to accommodate the chains during ligand association. The intercalation is known to be rapid (~ms) (33), occurring in pre-equilibrium to much slower side chain fitting (4,28). Therefore it is clear that DNA duplex destabilization, either by force or other factors (4,27–30), facilitates the rate limiting step of fitting and removing the side chains during both binding and unbinding of ActD by making the duplex more deformable. ActD shares this feature with so-called 'threading' intercalators that are being developed as a new class of anticancer drugs (26). While destabilization of the DNA duplex structure facilitates the kinetics of ActD binding as well as its equilibrium binding affinity, its final preferred bound state is always to two, not just one DNA strand. This is consistent with earlier observations, in which ssDNA oligomers fold back on themselves to form mismatched duplexes upon ActD binding (10).

The efficient anticancer activity of ActD is due to its ability to inhibit DNA transcription and replication at low (~10 nM) concentrations, with a lower toxicity for normal cells than cancer cells (34). The concentration of DNA-binding sites for ActD in the nucleus is high and variable, as it depends on DNA accessibility within chromatin, which changes dramatically during the cell cycle. However, the effective DNA-binding site concentration always exceeds the K_d ~1 μM for the ActD binding to B-form dsDNA, such that all available ActD will always be DNA-bound. In normal cells with relatively low transcriptional activity, most of the DNA exists in its normal B-form duplex. In such cells, most of the ActD will be absorbed by the few 'alternative' or defective DNA structures, and will likely not strongly alter normal DNA transcription. In contrast, in cancerous cells with greatly elevated transcriptional activity, a majority of the ActD will accumulate within helicase-unwound DNA transcription bubbles. These sites have an especially high ActD-binding affinity, as the binding to such sites occurs 100-fold faster than to B-form dsDNA, due to duplex destabilization by the helicase. An additional preference of ActD for these sites may be ensured by their steric accessibility within the chromatin. At the same time, ActD unbinding after enzyme dissociation is expected to be as slow as its unbinding from stable B-form dsDNA, which should occur on the $\sim 1/k_{off}(0) \sim 1000$ s time scale. Therefore, transient DNA bubbles are not only favored by a 100-fold higher equilibrium ActD–DNA-binding affinity, but they are also kinetically selected and effectively locked on a time scale larger than typical biological processes.

In summary, our results suggest that the efficient anticancer activity of ActD is related to the strong facilitation of its DNA-binding kinetics by the elevated activity of dsDNA unwinding enzymes in cancerous cells, leading to an efficient transcription block by ActD that is effectively locked into the dsDNA structure after enzyme dissociation. This generic mechanism of activity explains the predominant effect of ActD on DNA transcription (18–20), and the low selectivity of ActD for different types of cancer, leading to its relatively high toxicity (34). Taken together with the large body of microscopic data on ActD–DNA interactions, these results may facilitate the development of anticancer drugs by exploiting the molecular properties of ActD responsible for this phenomenon while also lowering the toxicity of the drug.

The single molecule method developed here allows us to monitor ligand–DNA binding as a function of time, revealing both its kinetics and thermodynamics. Moreover, in the case of ActD this approach allows us to understand its preferred DNA-binding mode, the structural changes in DNA associated with its equilibrium binding, and the rate limiting deformations for the on and off processes. The approach developed in this work should be useful for studies of largely sequence non-specific and non-cooperative DNA-binding small molecules that bind and unbind DNA on a time scale >~10 s, while causing measurable changes in DNA length. As most slow binding processes are associated with significant structural changes in DNA, a majority of these processes are expected to lead to essential variation in DNA length, and will therefore be exponentially affected by the stretching force. In conclusion, we expect the method developed in this study to be a highly informative and general approach to the study of slow small molecule-DNA-binding processes.

SUPPLEMENTARY DATA

Supplementary Data are available at NAR Online: Supplementary Figures 1–9 and Supplementary References [35–37].

ACKNOWLEDGEMENTS

The authors acknowledge valuable discussions with Henry Sobell and Michael Waring.

FUNDING

National Institutes of Health (GM-072462); the National Science Foundation (MCB-0744456). Funding for open access charge: National Institutes of Health (GM-072462).

Conflict of interest statement. None declared.

REFERENCES

1. Kersten,W., Kersten,H. and Rauen,H.M. (1960) Action of nucleic acids on the inhibition of growth by actinomycin of Neurospora crassa. *Nature*, **187**, 60–61.
2. Waksman,S.A. and Woodruff,H.B. (1942) Selective antibiotic action of various substances of microbial origin. *J. Bacteriol.*, **44**, 373–384.
3. Farber,S., D'Angio,G., Evans,A. and Mitus,A. (1960) Clinical studies of Actinomycin D with special reference to Wilms' tumor in children. *Ann. NY Acad. Sci.*, **89**, 421–424.
4. Müller,W. and Crothers,D.M. (1968) Studies of the binding of actinomycin and related compounds to DNA. *J. Mol. Biol.*, **35**, 251–290.
5. Sobell,H.M., Jain,S.C., Sakore,T.D. and Nordman,C.E. (1971) Stereochemistry of actinomycin–DNA binding. *Nature. New Biol.*, **231**, 200–205.
6. Sobell,H.M. and Jain,S.C. (1972) Stereochemistry of actinomycin binding to DNA. II. Detailed molecular model of actinomycin-DNA complex and its implications. *J. Mol. Biol.*, **68**, 21–34.

7. Takusagawa,F., Dabrow,M., Neidle,S. and Berman,H.M. (1982) The structure of a pseudo intercalated complex between actinomycin and the DNA binding sequence d(GpC). *Nature*, **296**, 466–469.
8. Lian,C., Robinson,H. and Wang,A.H.-J. (1996) Structure of Actinomycin D bound with (GAAGCTTC)2 and (GATGCTTC)2 and its binding to the (CAG)n:(CTG)n triplet sequence as determined by NMR analysis. *J. Am. Chem. Soc.*, **118**, 8791–8801.
9. Wadkins,R.M. and Jovin,T.M. (1991) Actinomycin D and 7-aminoactinomycin D binding to single-stranded DNA. *Biochemistry*, **30**, 9469–9478.
10. Chen,F.M., Sha,F., Chin,K.H. and Chou,S.H. (2004) The nature of actinomycin D binding to d(AACCAXYG) sequence motifs. *Nucleic Acids Res.*, **32**, 271–277.
11. Zhou,X., Shen,Z., Li,D., He,X. and Lin,B. (2007) Study of interactions between actinomycin D and oligonucleotides by microchip electrophoresis and ESI-MS. *Talanta*, **72**, 561–567.
12. Rill,R.L. and Hecker,K.H. (1996) Sequence-specific actinomycin D binding to single-stranded DNA inhibits HIV reverse transcriptase and other polymerases. *Biochemistry*, **35**, 3525–3533.
13. Wadkins,R.M., Jares-Erijman,E.A., Klement,R., Rüdiger,A. and Jovin,T.M. (1996) Actinomycin D binding to single-stranded DNA: sequence specificity and hemi-intercalation model from fluorescence and 1H NMR spectroscopy. *J. Mol. Biol.*, **262**, 53–68.
14. Alexopoulos,E., Jares-Erijman,E.A., Jovin,T.M., Klement,R., Machinek,R., Sheldrick,G.M. and Uson,I. (2005) Crystal and solution structures of 7-amino-actinomycin D complexes with d(TTAGBrUT), d(TTAGTT) and d(TTTAGTTT). *Acta Crystallogr. D Biol. Crystallogr.*, **61**, 407–415.
15. Bittman,R. and Blau,L. (1975) Stopped-flow kinetic studies of actinomycin binding to DNAs. *Biochemistry*, **14**, 2138–2145.
16. Robinson,H., Gao,Y.G., Yang,X., Sanishvili,R., Joachimiak,A. and Wang,A.H. (2001) Crystallographic analysis of a novel complex of actinomycin D bound to the DNA decamer CGATC GATCG. *Biochemistry*, **40**, 5587–5592.
17. Chen,F.M., Sha,F., Chin,K.H. and Chou,S.H. (2003) Unique actinomycin D binding to self-complementary d(CXYGGCCY'X'G) sequences: duplex disruption and binding to a nominally base-paired hairpin. *Nucleic Acids Res.*, **31**, 4238–4246.
18. Reich,E., Franklin,R.M., Shatkin,A.J. and Tatum,E.L. (1961) Effect of actinomycin D on cellular nucleic acid synthesis and virus production. *Science*, **134**, 556–557.
19. Goldberg,I.H. and Rabinowitz,M. (1962) Actionmycin D inhibition of deoxyribonucleic acid-dependent synthesis of ribonucleic acid. *Science*, **136**, 315–316.
20. Sobell,H.M. (1985) Actinomycin and DNA transcription. *Proc. Natl Acad. Sci. USA*, **82**, 5328–5331.
21. Chaurasiya,K.R., Paramanathan,T., McCauley,M.J. and Williams,M.C. (2010) Biophysical characterization of DNA binding from single molecule force measurements. *Phys. Life Rev.*, **7**, 299–341.
22. Vladescu,I.D., McCauley,M.J., Nuñez,M.E., Rouzina,I. and Williams,M.C. (2007) Quantifying force-dependent and zero-force DNA intercalation by single-molecule stretching. *Nat. Methods*, **4**, 517–522.
23. Shokri,L., Rouzina,I. and Williams,M.C. (2009) Interaction of bacteriophage T4 and T7 single-stranded DNA-binding proteins with DNA. *Phys. Biol.*, **6**, 025002.
24. Shokri,L., Marintcheva,B., Richardson,C.C., Rouzina,I. and Williams,M.C. (2006) Single molecule force spectroscopy of salt-dependent bacteriophage T7 gene 2.5 protein binding to single-stranded DNA. *J. Biol. Chem.*, **281**, 38689–38696.
25. Pant,K., Karpel,R.L., Rouzina,I. and Williams,M.C. (2005) Salt dependent binding of T4 gene 32 protein to single and double-stranded DNA: single molecule force spectroscopy measurements. *J. Mol. Biol.*, **349**, 317–330.
26. Paramanathan,T., Westerlund,F., McCauley,M.J., Rouzina,I., Lincoln,P. and Williams,M.C. (2008) Mechanically manipulating the DNA threading intercalation rate. *J. Am. Chem. Soc.*, **130**, 3752–3753.
27. Krugh,T.R. (1972) Association of actinomycin D and deoxyribodinucleotides as a model for binding of the drug to DNA. *Proc. Natl Acad. Sci. USA*, **69**, 1911–1914.
28. Shafer,R.H., Burnette,R.R. and Mirau,P.A. (1980) Spectroscopic analysis of the equilibrium and kinetic DNA binding properties of several actinomycin analogs. *Nucleic Acids Res.*, **8**, 1121–1132.
29. Wadkins,R.M., Tung,C.S., Vallone,P.M. and Benight,A.S. (2000) The role of the loop in binding of an actinomycin D analog to hairpins formed by single-stranded DNA. *Arch Biochem. Biophys.*, **384**, 199–203.
30. Vekshin,N. (2011) Melting of DNA-actinomycin clusters. *J. Biochem.*, **149**, 601–607.
31. White,R.J. and Phillips,D.R. (1988) Transcriptional analysis of multisite drug-DNA dissociation kinetics: delayed termination of transcription by actinomycin D. *Biochemistry*, **27**, 9122–9132.
32. Wolf,L.K., Gao,Y. and Georgiadis,R.M. (2007) Kinetic discrimination of sequence-specific DNA-drug binding measured by surface plasmon resonance imaging and comparison to solution-phase measurements. *J. Am. Chem. Soc.*, **129**, 10503–10511.
33. Bresloff,J.L. and Crothers,D.M. (1975) DNA-ethidium reaction kinetics: demonstration of direct ligand transfer between DNA binding sites. *J. Mol. Biol.*, **95**, 103–123.
34. Takusagawa,F., Carlson,R.G. and Weaver,R.F. (2001) Anti-leukemia selectivity in actinomycin analogues. *Bioorg. Med. Chem.*, **9**, 719–725.
35. Vladescu,I.D., McCauley,M.J., Nuñez,M.E., Rouzina,I. and Williams,M.C. (2007) Quantifying force-dependent and zero-force DNA intercalation by single-molecule stretching. *Nat. Methods*, **4**, 517–522.
36. Vladescu,I.D., McCauley,M.J., Rouzina,I. and Williams,M.C. (2005) Mapping the phase diagram of single DNA molecule force-induced melting in the presence of ethidium. *Phys. Rev. Lett.*, **95**, 158102.
37. Mihailovic,A., Vladescu,I., McCauley,M., Ly,E., Williams,M.C., Spain,E.M. and Nunez,M.E. (2006) Exploring the interaction of ruthenium(II) polypyridyl complexes with DNA using single-molecule techniques. *Langmuir*, **22**, 4699–4709.